Journal of Inorganic and Organometallic Polymers and Materials (2022) 32:4237–4249
https://doi.org/10.1007/s10904-022-02423-9

# Hydrophobic $Al_2O_3/SiO_2$/PDMS Composite Coatings for Anti-corrosion Application of 304 Stainless-Steel

Xuening Sun[1] · Jing Xie[2] · Jinfeng Zhang[2] · Min Sang[2] · Yanli Li[2] · Pei Lyu[1] · Dongzhi Chen[1,2] · Hongjun Zhou[3]

Received: 13 April 2022 / Accepted: 18 June 2022 / Published online: 19 July 2022
© The Author(s), under exclusive licence to Springer Science+Business Media, LLC, part of Springer Nature 2022

## Abstract

Polymer coatings for steel anticorrosion are usually susceptible to damage by invading water, oxygen and chloride ions, therefore, it is still a great challenge to reduce these corrosive species to penetrate into coatings/substrate interface. Herein, new binary nanoparticles ($SiO_2$ and $Al_2O_3$) filled polydimethylsiloxanes (PDMS) composite coatings are developed for anti-corrosion application of 304 stainless-steel (304s) by combining with advantages of PDMS, silica and nano-$Al_2O_3$. Surface wettability, chemical compositions, microstructure, corroded morphologies, mechanical properties and thermal stability of the new PDMS composite coatings on the treated 304s sheets are studied, respectively. Subsequently, corrosion resistances of the 304s sheets treated with the composite coatings are also evaluated in corrosive medium (3.5 wt% NaCl solution) through potentiodynamic polarization tests and electrochemical impedance spectroscopy techniques, respectively. Interestingly, the $Al_2O_3/SiO_2$/PDMS composite coatings show superior mechanical properties, desirable stability and excellent corrosion resistance compared to the PDMS coating without adding $Al_2O_3$ nanoparticles. Moreover, the PDMS composite coating with $Al_2O_3$ content of 7.37% displays the best anticorrosion performance due to excellent barrier effect between the 304s sheets and corrosive species. This work not only presents a simple and cost-efficient approach to exploiting hydrophobic PDMS coatings by use of binary nanoparticles and PDMS matrix, but also paves the way to anticorrosive application for 304s.

**Keywords** Nanoparticles · Composite coatings · Surface treatment · Hydrophobicity · Anti-corrosion

## 1 Introduction

Steel is one of the most fundamental and valuable resources for one nation because it has extensively been used in many areas including pipelines, shipping, biomedical implants, rail transport and infrastructure construction owing to outstanding processability, high tensile, recyclability and low cost. However, mild steel is vulnerable to corrosion when exposed in ambient environment, which causes huge economy losses and potential environment hazards [1–7]. To delay the steel corrosion, various measures have been taken such as passivating the metal substrate [8], cathodic protection [9, 10], surface protective coatings [11, 12], corrosion inhibitors [13], and so forth. In earlier literature, hexavalent chromium coatings have been employed to protect metals from corrosions effectively [14], but they are prohibited worldwide to use due to high toxicity and carcinogenicity [15]. Among the mentioned-above anti-corrosion technologies, the use of polymer coatings to inhibit steel corrosion from water and oxygen has hitherto been the most economical, promising and convenient way.

Over the past decade, polymeric coatings have received considerable attention to metal anticorrosion from industry and academia [16–22], including polydopamine [16], polyaniline [23], epoxy [24–26], polylactide [27], PMMA and so forth [28]. However, only single polymer coatings are hard to achieve desirable comprehesive performances during real-life application. Furthermore, the polymer coatings are usually susceptible to damage by invading water, oxygen and ions,

✉ Dongzhi Chen
chdozh_2008@163.com

✉ Hongjun Zhou
zhou73262811@126.com

[1] State Key Laboratory of New Textile Materials & Advanced Processing Technology, Wuhan Textile University, Wuhan 430073, People's Republic of China

[2] School of Materials Science and Engineering, Wuhan Textile University, Wuhan 430200, People's Republic of China

[3] Shanxi Zhendong Pharmaceutical Co., Ltd, Zhendong Science and Technology Park, Changzhi 047100, People's Republic of China

it is still a great challenge to prevent these corrosive media from permeating into the coatings/steel interface. To further improve required performance of polymer coatings, a variety of inorganic nanoparticles, including titania, zinc oxide, silica, $Fe_3O_4$ and so forth, have been added as pigments or reinforcing fillers [23, 24, 29–34]. Among these nanoparticles, nano-$Al_2O_3$ is an ideal alternative for protective coatings owing to low cost, low electron conductance, high hardness [35–38]. Therefore, these merits of alumina nanoparticles motivate us to fabricate new durable functional coatings.

It is well-documented that the hydrophobic properties of composite coatings play a vital role in anticorrosion applications. Generally, hydrophobic surface can be created by combining the micro-nano structures with low-surface-energy coatings. In recent years, some alternatives for the forementioned polymeric matrices such as some silanes and siloxanes, have been used as alloy anticorrosive coatings due to excellent hydrophobicity [39–42]. In particular, PDMS are made up of the -Si–O-Si- main chains with high bond energy and the $CH_3$ side groups with free rotatability, endowing PDMS with excellent thermal stability and superior hydrophobicity. Hence, PDMS should be one of desirable polymeric matrices for developing a variety of organic/inorganic composite functional coatings. However, unfilled PDMS exhibit poor mechanical properties due to inherent weak interaction between PDMS chains [43, 44]. Many efforts have been devoted to the enhancement on mechanical properties of PDMS composites during practical applications [45–49]. It is well-known that nano-silica is indispensable reinforcing filler for mechanical enhancement of PDMS matrix due to low costs, excellent chemical stability and superior compatibility. Moreover, some reports disclose that nano silica can also be used as corrosion inhibitors for stainless steel [28, 50–56]. Therefore, it is highly desirable to explore hydrophobic PDMS composite coatings for anticorrosion applications of steel by employing nano silica.

Hence, in this work, new binary nanoparticles ($SiO_2$ and $Al_2O_3$) filled polydimethylsiloxanes (PDMS) composite anticorrosive coatings for stainless steel were developed by combining with advantages of PDMS, silica and nano-$Al_2O_3$. The hydrophobicity, chemical composition, microstructure, corrosive morphologies, mechanical properties and stability of the new PDMS composite coatings with binary particles filled on surface of the treated 304s sheets were characterized, respectively. The anticorrosion performances of the $Al_2O_3/SiO_2$/PDMS composite coatings are the main focuses of this paper.

## 2 Experimental Section

### 2.1 Materials

Polished 304s sheets with size of 2 cm × 2 cm × 0.2 cm were obtained from Wuhan Youmao Technology Co., Ltd., which were further ultrasonically cleaned in alcohol and acetone to wash away some contaminations, and the cleaned 304s sheets were used as the substrate. Hydrophilic fumed silica (AEROSIL 380, its size is 7 nm) was purchased from Shaoxing Lijie Chemical Co., Ltd. Hydroxyl-terminated polydimethylsiloxane (HPDMS) (viscosity, 5,000 cSt) was provided by Shandong Dayi Chemical Co. Ltd (Laiyang, Shandong Province). γ-aminopropyltriethoxysilane (99%) was obtained from Jiangsu Chenguang Coupling Agent Co., Ltd. Nano-aluminum oxide (α phase, about 30 nm) was supplied from Shanghai Chemical Industry Park (Shanghai, China). Petroleum ether (boiling range: 60 ~ 90 °C) and dibutyltin dilaurate (AR) were purchased from Sinopharm Chemical Reagent Co., Ltd. Deionized water was produced by a water purification apparatus (UPCIII40 L, Ulupure, Shanghai, China). All chemicals were used as received.

### 2.2 Fabrication of New $Al_2O_3/SiO_2$/PDMS Composite Coatings

30 g HPDMS was dissolved into 25 mL petroleum ether by mechanical stirring in a three-necked flask. After dissolution, 1.5 g fumed silica was stepwise added into the solution with stirring for 0.5 h. Then variable amounts of $Al_2O_3$ nanoparticles were dispersed into the $SiO_2$/PDMS mixture by mechanical stirring for 15 min to afford $Al_2O_3/SiO_2$/PDMS mixture. Finally, 6 g 3-(aminopropyl)triethoxysilane (APTES) and 0.226 g dibutyltin dilaurate (DBTDL) were respectively added to the dispersed mixture with mechanical stirring for another 15 min to afford the $Al_2O_3/SiO_2$/PDMS coatings. The $Al_2O_3/SiO_2$/PDMS composite coatings with different formulations are listed in Table 1. Afterward, the clean 304s sheets were immersed in the above $Al_2O_3/SiO_2$/PDMS composite coatings, and the immersed 304s sheets were picked up with tweezer. Then the $Al_2O_3/SiO_2$/PDMS composite coatings on surface of 304s sheets were cured at room temperature for 1 day, and their average thickness is 24 μm.

### 2.3 Characterization

Phase compositions of composite coatings on 304s sheets were characterized by powder X-ray diffraction spectra (XRD) using an UItima IV (Rigaku Corporation) with Cu $K_\alpha$ radiation ($\lambda = 0.15406$ nm) source (applied voltage

**Table 1** Recipe of the $Al_2O_3$/$SiO_2$/PDMS composite coatings

| Sample | Mass of HPDMS (g) | Mass of $SiO_2$ (g) | Mass of APTES (g) | Mass of $Al_2O_3$ (g) | Weight percentage of $Al_2O_3$ (%) | Mass of DBTDL (g) |
|---|---|---|---|---|---|---|
| SA-0 | 30 | 1.5 | 6 | 0 | 0.00 | 0.226 |
| SA-1 | 30 | 1.5 | 6 | 1.5 | 3.82 | 0.226 |
| SA-2 | 30 | 1.5 | 6 | 3 | 7.37 | 0.226 |
| SA-3 | 30 | 1.5 | 6 | 4.5 | 10.66 | 0.226 |

40 kV, current 40 mA) with a scanning speed of 5°/min and scanning step size 0.01°. Surface roughness of the PDMS composite coatings was measured by using an atomic force microscope (AFM, Dimension Icon, Bruker Company). Mechanical tests were performed on a universal testing machine (Instron 5967, UK, capacity 1 kN) at 25 °C according to measurement standard of silicone rubber. The tensile strength and modulus of the $Al_2O_3$/$SiO_2$/PDMS composites were measured by using a 20 mm/min cross-head speed. The dumbbell-shaped specimens were punched out of these cured sheets, at least five measurements for each sample were recorded for the $Al_2O_3$/$SiO_2$/PDMS composites. The static water contact angles (WCAs) of the samples were measured with 5 µL deionized water droplets at room temperature using a Dataphysics OCA15EC goniometer. An automatic injection pump was used to reside droplets on a substrate for analysis. At least five parallel measurements were made for each sample. The WCAs reported in this work were the average values of five measurements at different positions on each coating. The morphologies of the corroded coating surfaces were studied by scanning electron microscopy (SEM, JSM-IT500HR, JEOL Ltd, Tokyo, Japan) operated at a 10 kV accelerating voltage and sprayed gold at room temperature (25 °C). To increase their conductivity, all the specimens were sputtered with Au for 20 s before the SEM measurement. Elemental analyses were performed by energy dispersive X-ray spectroscopy (EDS) (Aztec Energy X-Max20, Oxford Instruments, Abingdon, UK) mapping on the surface of the $Al_2O_3$/$SiO_2$/PDMS coating. To investigate the anticorrosion performance of composite coatings, electrochemical impedance spectroscopy (EIS) measurements were performed on electrochemical workstation in 3.5 wt% sodium chloride solution (model CHI660E Shanghai Chenhua instruments Ltd., China). The platinum electrode, saturated calomel electrode and the treated 304s tainless-steel sheet (exposed surface area of 4 $cm^2$) are the counter electrode, reference electrode and working electrode, respectively. The amplitude of the sinusoidal signal was measured in the open circuit potential (OCP) mode, with the frequency ranging from $10^5$ to $10^{-2}$ Hz. Tafel polarization curves were recorded at a scan rate of 0.1 mV $s^{-1}$ from − 1000 to + 1000 mV. To ensure good reproducibility, each electrochemical test was repeated three times. The protection efficiency (η) of the composite coatings was calculated by the Eq. (1) [50],

$$\eta\% = 100 \times \left(I_{corr} - I_0\right)/I_{corr} \quad (1)$$

where $I_{corr}$ and $I_0$ are denoted the corrosion current values of 304s in the absence and presence of the coatings, respectively. To investigate thermal degradation behaviors of each sample, thermogravimetric analysis (TGA) was performed on Discovery TGA 55 (America Instruments) under gas flow of 50 mL/min. About 10 mg sample was heated in an $Al_2O_3$ crucible with 20 °C/min heating rate under nitrogen atmosphere from ambient temperature to 700 °C.

## 3 Results and Discussion

### 3.1 Hydrophobicity of the Treated 304s Sheets with PDMS Composite Coatings

It is well-documented that the hydrophobic properties of composite coatings play a vital role in anticorrosion applications. Hence, before corrosion, the hydrophobicity of the treated 304s sheets with PDMS composite coatings was assessed by measuring static WCA, respectively. Figure 1a clearly depicts that the WCA value of the pristine 304s sheet is 83.1 ± 6.5°, corroborating the surface of the polished 304s sheet is hydrophilic. But it increases to 119.3 ± 1.9° and 120.2 ± 1.9° after the polished 304s sheets were treated with the $SiO_2$/PDMS and the $Al_2O_3$/PDMS composite coatings, respectively. This increasing WCA value shows that the hydrophilic surface of 304s sheet transforms into hydrophobic one after treatment with the $SiO_2$/PDMS coating. As the $Al_2O_3$ nanoparticles were added, the WCA value of the treated 304s sheet with $Al_2O_3$/$SiO_2$/PDMS composite slightly increases to 123.5 ± 1.0°, which is slightly higher than those of the 304s sheets treated with the $SiO_2$/PDMS and the $Al_2O_3$/PDMS composite coatings. With an increasing amount of alumina nanoparticles, the WCA value of the treated 304s sheet further increases to 127.7 ± 1.0°, implying that the new $Al_2O_3$/$SiO_2$/PDMS composite coatings are favorable to preventing the penetration of water-soluble corrosive media. The increasing water-repellent barrier

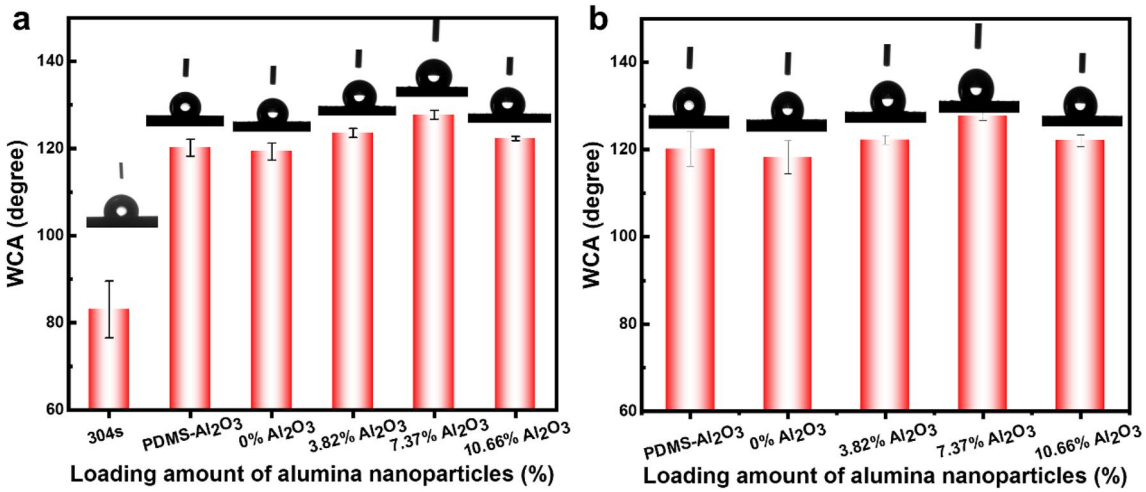


**Fig. 1** Static water contact angle (WCA) values of pristine 304s, 304s sheet treated with $Al_2O_3$/PDMS, and the 304s sheets treated by PDMS composite coatings with $Al_2O_3$ concentrations from 0 to 10.66%: a) before corrosion and b) after corrosion in 3.5 wt% NaCl for 24 h

property of the $Al_2O_3/SiO_2$/PDMS composite coatings is likely assigned to synergistic effect between hydrophobic PDMS matrix and the filled binary nanoparticles (silica and $Al_2O_3$). With a further increase in the loading amount of alumina nanoparticles, the WCA value of the treated 304s sheet begins to drop to $122.3 \pm 0.5°$, which should be due to the hydrophilic aggregations of alumina nanoparticles.

To further gain insight into water-repellent properties of the $Al_2O_3/SiO_2$/PDMS composite coatings, their WCAs were measured again after corroded in 3.5 wt% NaCl for 24 h. Figure 1b presents that after corrosion, the WCAs of the treated 304s sheets increase to $127.7 \pm 1.0°$ when the loading amount of alumina nanoparticles rise to 7.37%. With the further increase in the loading amount of alumina nanoparticles, the WCA of the treated 304s decreases to $122.0 \pm 1.4°$, corroborating the same changeable trend as that of the treated 304s sheet before corrosion. At the same time, there is no difference in the WCAs between before and after corrosion, verifying that the $Al_2O_3/SiO_2$/PDMS composite coatings on the 304s sheets possess outstanding water-repellent properties, as exhibited in Fig. 1a and b.

## 3.2 Compositions and Microstructure of the PDMS Composite Coatings on Surfaces of 304s Sheets

Surface compositions are an important factor to affect anti-corrosive performance of coatings. So, surface phase compositions of the representative samples were characterized by XRD. Figure 2a obviously displays $SiO_2$/PDMS composite coatings with and without alumina nanoparticles have two similar diffraction peaks located at around 12° and 22°, which should be ascribed to crystalline of cured PDMS and amorphous silica, respectively [57]. It is also found that the diffraction intensities of characteristic peaks at 50.7° and 74.7°, corresponding to austenite phases of 304s [37], become weaker after modification by $SiO_2$/PDMS and $Al_2O_3/SiO_2$/PDMS composite coatings compared to the pristine 304s. In the meantime, after treatment with $Al_2O_3/SiO_2$/PDMS coatings, some peaks located at 25.4°, 35.3°, 38.2° and 57.5° attributable to (012), (104), (110) and (116) crystal planes of α-$Al_2O_3$ are still discernible, respectively, indicating that the composite coatings were successfully coated on the surface of 304s sheets.

To further observe micro/nano structures of the PDMS composite coatings on 304s sheets, the surface roughness of the 304s sheets treated with the PDMS composite coatings was evaluated by root mean square (RMS). It is interesting to find that the RMS value of the representative 304s sheet treated with $SiO_2$/PDMS composite coatings is only 15.8 nm, some irregular pillars (less than 1 μm wide) and sphere humps (around 2 μm wide) due to irregular agglomerated silica and assembly silica are clearly observed, respectively, contributing the increasing surface roughness, as shown in Fig. 2b. With the loading amount of nano $Al_2O_3$, more and more irregular pillars are observed strikingly on surfaces of the treated 304s sheets, as shown in Fig. 2c and d. As the 304s sheet was treated with $SiO_2$/PDMS composite coating containing 7.33% alumina nanoparticles, its RMS value increases to 19.5 nm. With a further increase in the loading amount of alumina nanoparticles, the RMS value of the treated 304s sheet keeps rising to 25.7 nm, confirming that the surface the treated 304s sheet become rough with the loading amount of alumina nanoparticles. The increasing surface roughness in Figs. 2b ~ d is attributable to the agglomerations of the increasing loading nanoparticles, verifying that micro/nano structures have been successfully constructed on the 304s sheet surfaces by immersion in the $Al_2O_3/SiO_2$/PDMS composite coatings.

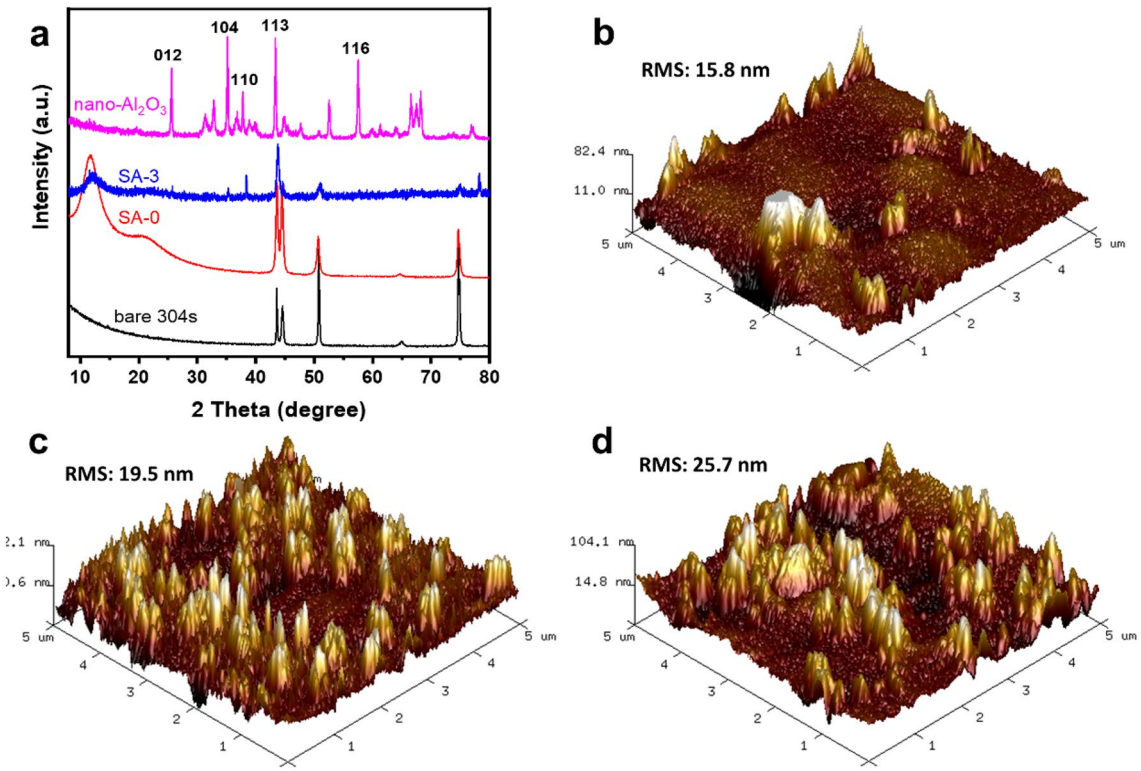


**Fig. 2** **a** XRD patterns of the representative samples, AFM images of the 304s sheets treated with PDMS composite coatings: **b** SA-0, **c** SA-2, and SA-3

Before coating, the bare 304s sheet apparently exhibits some scratches, many pores and holes are available on its surface. After treatment, the $SiO_2$/PDMS coating covers over the surface of the polished 304s sheet, and some protrusions are formed, as shown in Fig. 3a and b. The inset image on the left corner in Fig. 3b clearly demonstrates that the newly formed protrusions are aggregations that are made up of the spherical silica with uniform size (around 2 μm) due to self-assembly of dispersed silica in PDMS matrix, corresponding to the results in Fig. 2b. After compounding $Al_2O_3$ particles, the irregular aggregated $Al_2O_3$ particles embedded into $SiO_2$/PDMS coatings appear. At the same time, Fig. 3c shows that many bumps with size of around 50 μm are formed due to poor dispersibility when the amount of $Al_2O_3$ particles increased to 7.37%, which confirms that the surface of the treated 304s sheet become rougher as compared to that of treatment with only $SiO_2$/PDMS coating, as proposed in Scheme 1. As the amount of $Al_2O_3$ particles increased to 10.66%, many protrusions and bumps with large size of around 100 μm, nonwetting microparticles and gap are observable, respectively, as revealed in Fig. 3d. Although the protrusions and bumps can make surface of the $Al_2O_3$/$SiO_2$/PDMS composite coating on 304s sheet rough, they simultaneously cause dispersive defects on the surface of composite coating such as gaps.

Subsequently, surface chemical compositions of the representative 304s sheet (Figure S1a) treated with the composite coating containing 7.37% $Al_2O_3$ nanoparticles were characterized. Figure S1b clearly shows that five elements such as C, N, O, Al and Si are found with content of 39.46%, 2.94%, 26.24%, 0.98% and 30.38%, respectively. Figure S1c–S1g distinctly display that C, O, Si and N are uniformly distributed in the $Al_2O_3$/$SiO_2$/PDMS composite coating, only Al element presents some irregular domains, suggesting that alumina nanoparticles were agglomerated to some extent in the $Al_2O_3$/$SiO_2$/PDMS composite coating after compounding.

In order to evaluate corrosion resistance of the composite coatings, the coated 304s sheets were exposed in 3.5 wt% NaCl solution for 24 h, and their corroded morphologies were also observed. As no alumina particles were added, many protrusions are observed clearly in Fig. 4a. However, some sodium chloride crystals circled in Fig. 4a are found and stick on the surface of the $SiO_2$/PDMS coating, indicating that the electrolyte could permeate into the $SiO_2$/PDMS coating. After adding alumina nanoparticles, many irregular protrusions and some gaps are observable on the surfaces of the corroded $Al_2O_3$/$SiO_2$/PDMS composite coating, respectively. In this case, the gaps should be the occupied space of the protrusions and aggregates resulting from

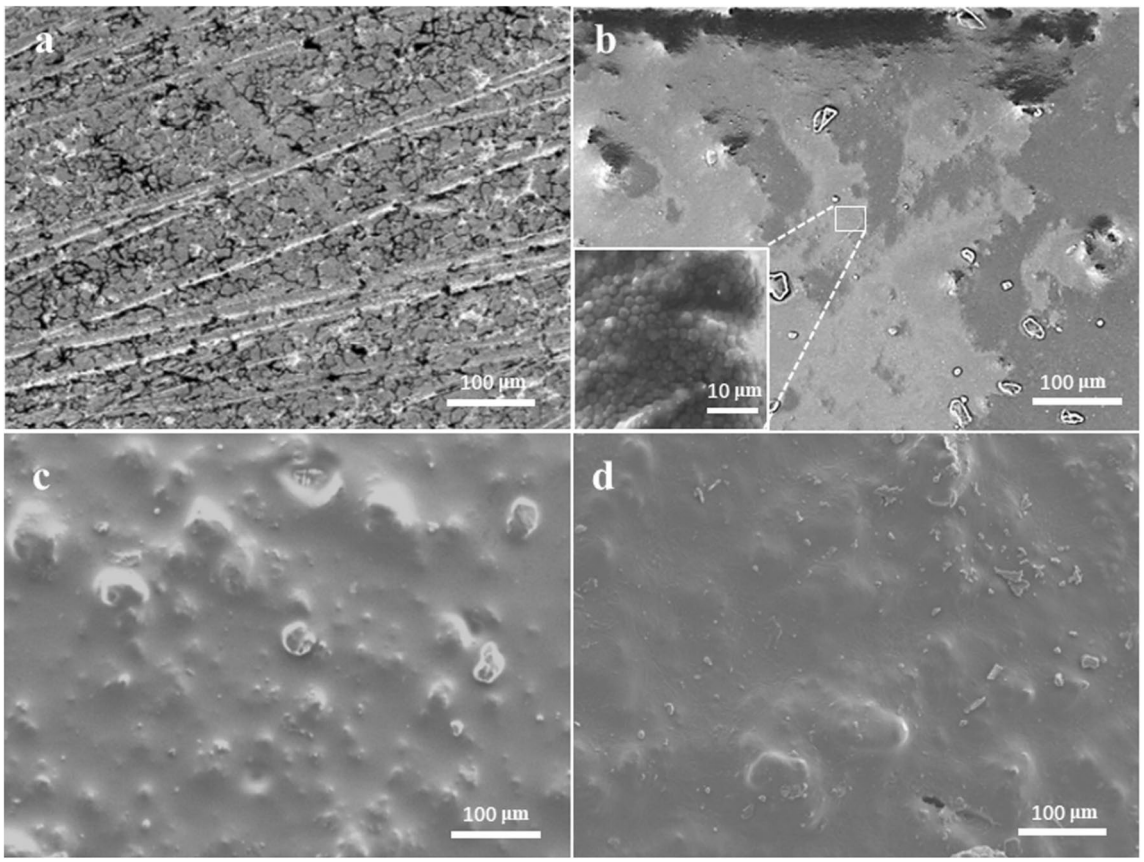


**Fig. 3** Surface SEM images of select samples: **a** bare 304s sheet and **b** the 304s sheet coated by SA-0, the inset on the left corner is the magnifying views of the white selected domains and **c** the 304s sheet coated with SA-2, **d** the 304s sheet coated with SA-3

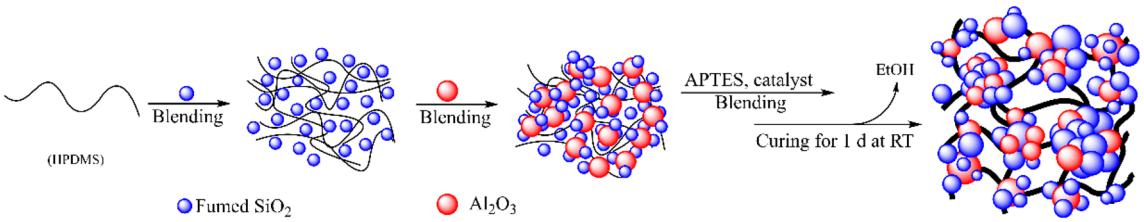


**Scheme 1** Proposed crosslinking mechanism of the composite coatings combined with the PDMS, fumed silica and $Al_2O_3$ nanoparticles

nonuniformly-dispersed binary particles. After electrolyte corrosion, the particles with dispersive imperfections are dissolved into aggressive aqueous electrolyte, and the occupied space is released, as shown in Fig. 4b. As the weight percent of the alumina nanoparticles increased to 7.37%, no hole, or gap, or sodium chloride crystal can be found on the surface of the treated 304s sheet after electrolyte corrosion, suggesting that the aqueous electrolyte cannot wet the surface of the $Al_2O_3/SiO_2$/PDMS composite coating, conferring the composite coating with excellent anticorrosive properties, as shown in Fig. 4c. The excellent resistance to electrolyte of $Al_2O_3/SiO_2$/PDMS composite coating could be ascribed to synergistic dispersive effect of the binary nanoparticles, which seems to prevent electrolyte from corrosion. With further increment of the alumina nanoparticles, more and more holes are observed on the surface of the composite coating after corrosion as compared to those of the composite coatings with low loading amount of alumina nanoparticles (e.g. 3.82% and 7.37%), as displayed in Fig. 4d. At the same time, the shrinkage phenomenon of the composite coating is observable when the content of alumina nanoparticles increased to 10.66%, as shown in magnifying inset on the right corner in Fig. 4d. Two factors should be mainly taken into account for the formed holes and the shrinkage phenomenon of the composite coatings. On one hand, hydroxyl ions are easily formed during electrochemical corrosion [36],

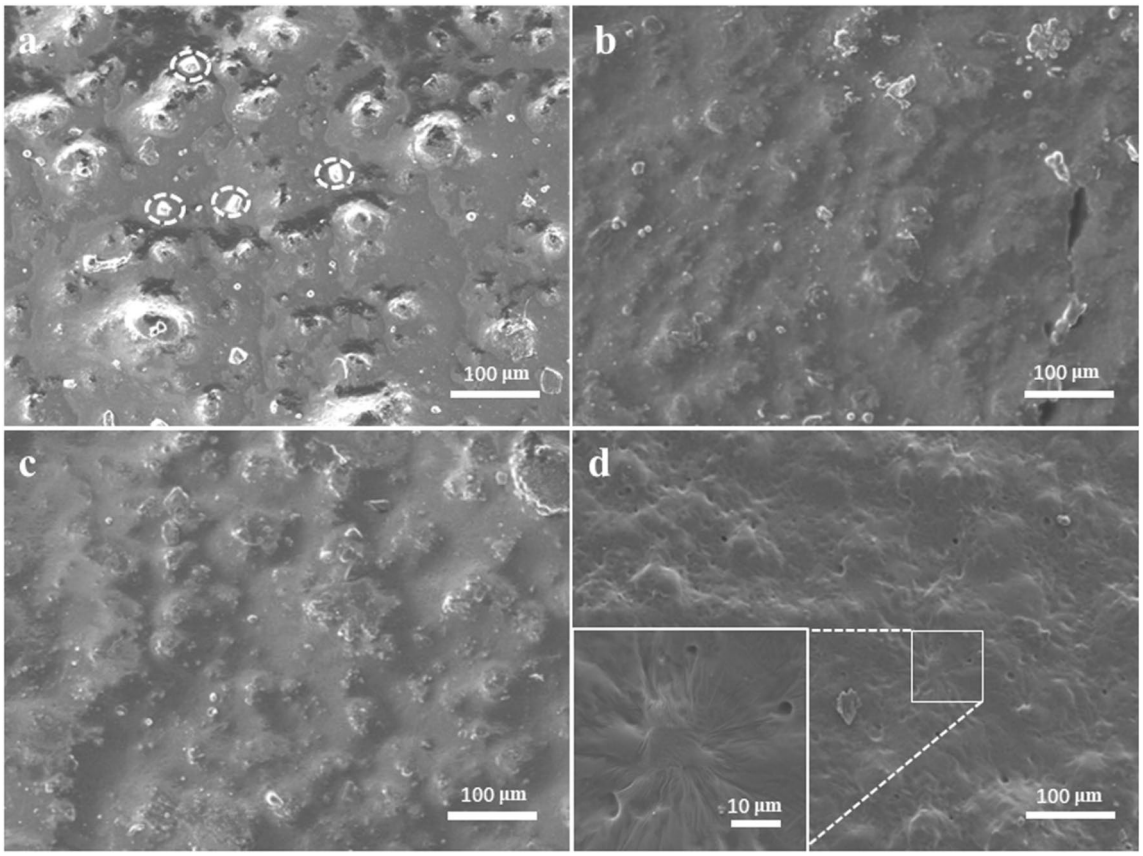


**Fig. 4** SEM images of the select 304s sheets coated with: **a** SA-0, and **b** SA-1, **c** SA-2, **d** SA-3, after corroding in 3.5 wt% NaCl aqueous solution for 24 h, the inset on the right corners is the magnifying views of the white selected domain

which create alkaline environment and catalyze hydrolytic degradation of the cured PDMS chains. The catalytic degradation results in the shrinkage phenomenon of the composite coatings. On the other hand, hydroxyl ions can intrude into the composite coatings through dispersion defects and gaps, and react with alumina aggregates. This makes alumina aggregates dissolve into electrolyte, leading to formation of many micro-holes. Collectively, the $SiO_2$/PDMS composite coating with 7.37% of alumina nanoparticles exhibits the optimum corrosion resistance to electrolyte when applied to surface treatment of the 304s sheets.

### 3.3 Mechanical Properties of the PDMS Composites

Mechanical properties are vital parameters of the $Al_2O_3$/$SiO_2$/PDMS composites during practical application. Hence the effect of the loading amount of $Al_2O_3$ nanoparticles on mechanical properties of the $Al_2O_3$/$SiO_2$/PDMS composites was investigated thoroughly. The representative strain–stress curves in uniaxial tension for the $Al_2O_3$/$SiO_2$/PDMS composites are shown in Fig. a. The tensile strength of $Al_2O_3$/$SiO_2$/PDMS composites is enhanced from 0.28 MPa to 0.40 MPa with the loading amount of $Al_2O_3$, which is higher than that of 0.22 MPa for the $SiO_2$/PDMS compo5site. In the meantime, the elongation at break of the $Al_2O_3$/$SiO_2$/PDMS composites also increases to 450% with an increase in amount of $Al_2O_3$ nanoparticles, which is longer than 220% for the $SiO_2$/PDMS composite, implicating that excellent elastic property for the $Al_2O_3$/$SiO_2$/PDMS composites. Additionally, Young's modulus of the $Al_2O_3$/$SiO_2$/PDMS composites is improved from $0.32 \pm 0.01$ MPa to $0.46 \pm 0.05$ MPa with an increase in loading mass of alumina nanoparticles, which is higher as compared to $0.30 \pm 0.02$ MPa, as shown in Fig. 5b. The reinforcing tensile properties of the $Al_2O_3$/$SiO_2$/PDMS composites should be ascribed to synergistic dispersion between silica and alumina nanoparticles in PDMS matrix.

### 3.4 Thermal Stability of the PDMS Composite Coatings

The stability of coatings is also an important criterion in assessing their performance before application. Thermal degradative behavior of the PDMS composite coatings was examined, and their TGA and DTG curves are presented in Fig. 6. It is clear to find that initial degradation (5%

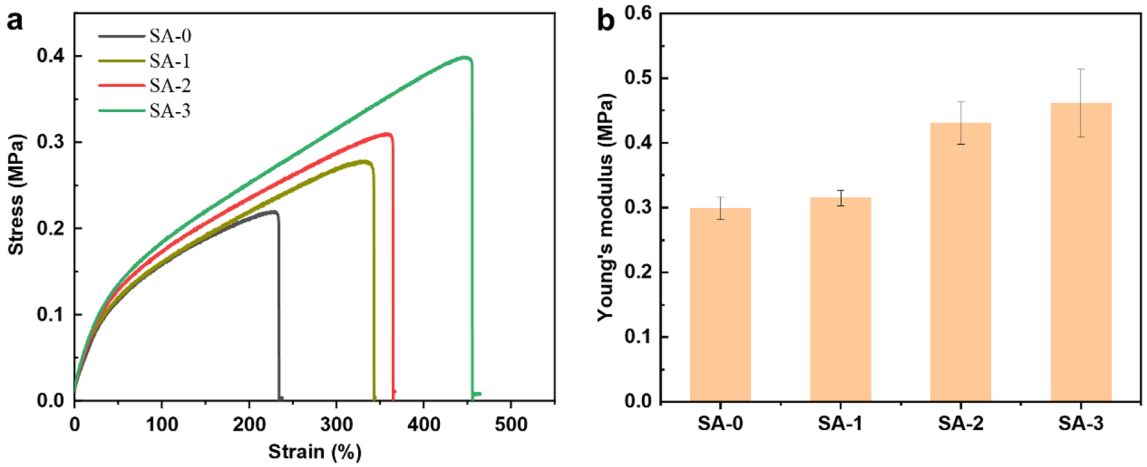


**Fig. 5** Tensile properties of the $SiO_2$/PDMS and $Al_2O_3/SiO_2$/PDMS composites: **a** stress versus strain, and **b** Young's modulus

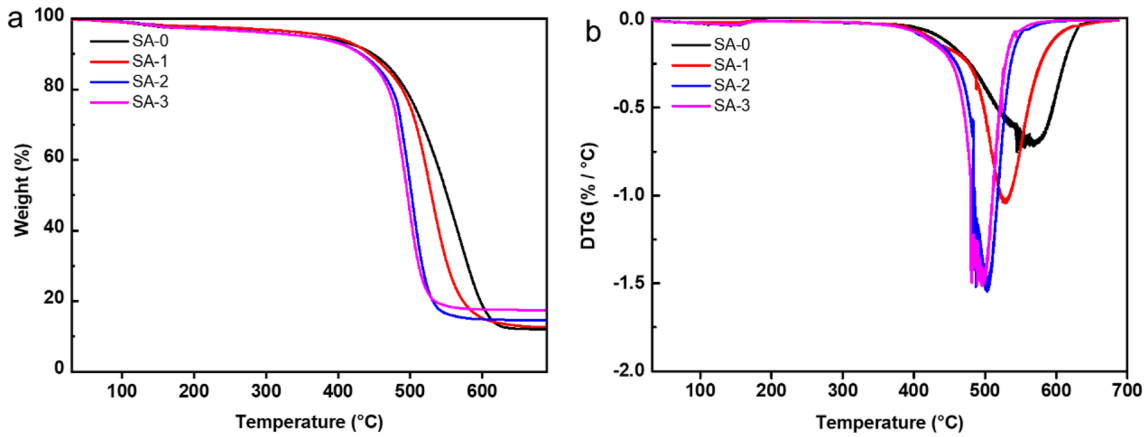


**Fig. 6** **a** TGA and **b** DTG profile for $SiO_2$/PDMS and $Al_2O_3/SiO_2$/PDMS composite coatings in nitrogen atmosphere

loss) temperature of the composite coatings is improved to 388.2 °C when adding amount of alumina nanoparticles was 3.82%, which is higher than 356.5 °C for the $SiO_2$/PDMS coating without alumina nanoparticles. The increasing initial temperature of the PDMS composite coatings is likely attributable to synergy between silica and alumina nanoparticles. Unfortunately, with a further increase in the loading amount of alumina nanoparticles, the initial decomposing temperature of the PDMS composite coatings is lowered to 354.3 °C. Similarly, the temperature for 50% weight loss of the PDMS composite coatings decrease from 551.3 to 496.9 °C with an increase in adding amount of alumina nanoparticles, as shown in Fig. 6a and Table 2. Moreover, the temperature for the maximum degradation rate of the composite coatings remarkably decreases from 570.5 °C to 492.9 °C with an increase in loading amount of alumina nanoparticles, as demonstrated in Fig. 6b and Table 4. Additionally, residual yield of the PDMS composite coatings is progressively improved with the increase in loading amount of alumina nanoparticles. The decreasing degradation temperature of the composite coatings should be assigned to catalytic decomposition of many hydroxyl groups available on surface of protrusions and bumps made up of silica and alumina nanoparticles [58, 59].

**Table 2** Characteristic parameters for thermal degradation of PDMS composite coatings in nitrogen atmosphere

| Sample | Temperature for different mass loss (°C) | | | Residual yield (%) |
|---|---|---|---|---|
| | 5% | 50% | At maximal rate | |
| SA-0 | 356.5 | 551.3 | 570.5 | 12.0 |
| SA-1 | 388.2 | 529.7 | 527.9 | 12.7 |
| SA-2 | 356.0 | 502.0 | 503.3 | 14.6 |
| SA-3 | 354.3 | 496.4 | 492.9 | 17.5 |

Additionally, the effect of the treated temperature on the wettability of the $Al_2O_3/SiO_2$/PDMS coatings on the 304s sheets was also evaluated. Figure S2 presents the change of the WCA value for the representative 304s sheet (SA-2) under different temperature treatment for 1 h. It is noteworthy that the WCA value for the representative specimen slightly decreases from $127.5 \pm 0.9°$ to $121.9 \pm 2.7°$ when the treatment temperature is 50 °C. With a further increment of the treatment temperature, the WCA value always keeps around 122°, indicating that the $Al_2O_3/SiO_2$/PDMS coating possesses excellent stability.

### 3.5 Anti-corrosion Performance of the 304s Sheets Treated with PDMS Composite Coatings

The anticorrosion performance of the PDMS composite coatings were evaluated by EIS method. Interestingly, on the Bode plots, the impedance modulus values of all the PDMS composite coatings coated 304s from high frequency to low frequency region is far higher as compared with the bare 304s sheet, implying that excellent barrier properties of the PDMS composite coatings against corrosive electrolyte. Moreover, the value of impedance modulus |Z| at the lowest frequency (f = 0.01 Hz) is commonly employed to evaluate the anticorrosion performance of the coatings [60]. After the 304s sheet was coated with $SiO_2$/PDMS, the value of impedance modulus at the lowest frequency increases from 5.9 to 901.6 kΩ $cm^2$, indicating enhancing corrosion protection for 304s sheet. More notably, the value of impedance modulus at the lowest frequency increases from 1390 to 2168 kΩ $cm^2$ firstly, and then drastically drop to 207.9 kΩ $cm^2$ with an increase in the content of alumina nanoparticles, indicating that with an increase in the loading content of nano $Al_2O_3$ increases, the overall corrosion resistance of the $Al_2O_3/SiO_2$/PDMS composite coating increases first and then decreases, as shown in Fig. 7a. In this case, the increase in impedance modulus for the PDMS composite coatings can be attributable to the hydrophobicity of PDMS matrix and synergistic barrier effects between silica and alumina nanoparticles well-dispersed in PDMS composite coating. Addition of an appropriate amount of nano $Al_2O_3$ favorably results in synergistic effect between silica and alumina nanoparticles so that the coating can keep excellent corrosion resistance.

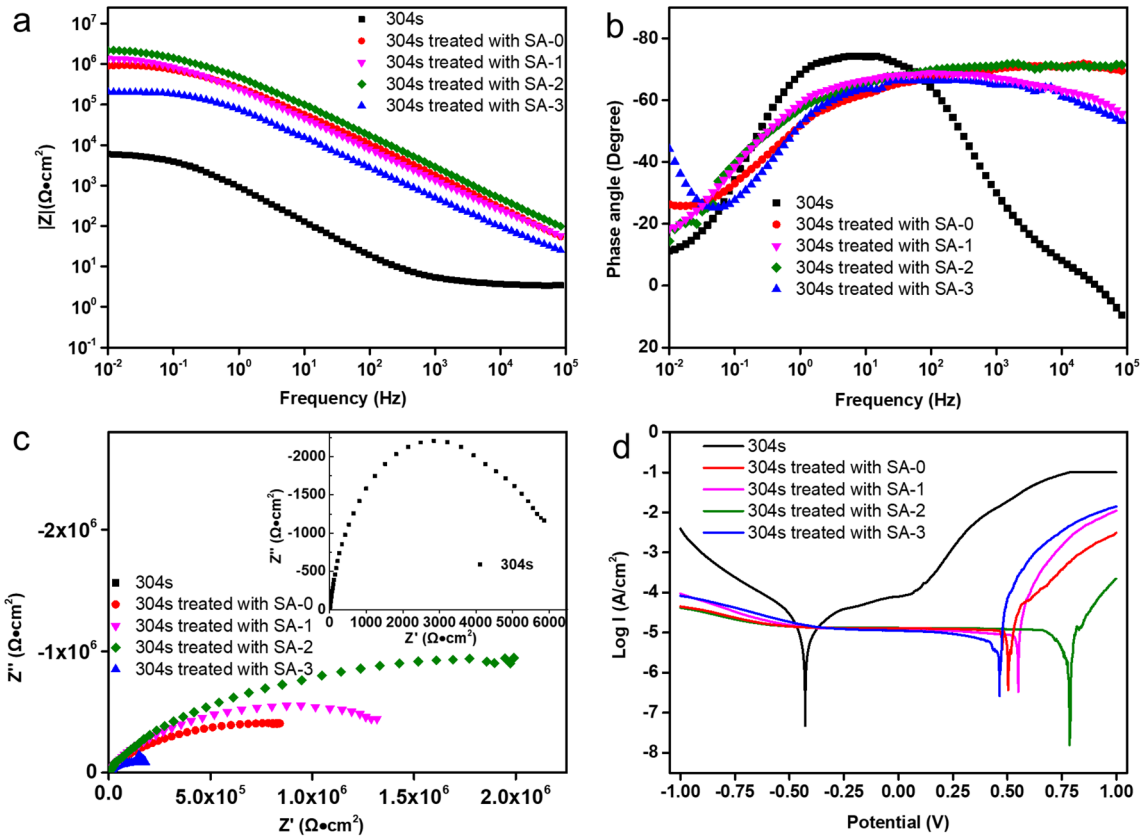


**Fig. 7** Bode plots of the uncoated and coated 304s with PDMS composite coatings after immersion in 3.5 wt. % NaCl solution for 24 h: a) impedance modulus |Z| versus frequency and b) phase angle versus frequency; c) Nyquist plots of the uncoated and coated samples after 24 h immersion in 3.5 wt. % NaCl solution and d) Tapel polarization curves of the pristine 304s and coated 304s with PDMS composite coatings after immersion in 3.5 wt. % NaCl solution for 24 h

But excessive addition of nano $Al_2O_3$ is beneficial to enhancing the interaction between micro-nano particles, leading to more dispersive defects in PDMS matrix. The dispersive defects in PDMS matrix are usually caused by the increasing number of the protrusions and bumps due to the agglomerated hydrophilic silica and alumina nanoparticles. The protrusions and bumps contain a large amount of Si–OH and Al–OH groups, which can absorb water, and are susceptibly invaded by aggressive species (water, oxygen and chloride ions), causing the impedance modulus to drop rapidly [56].

Figure 7b shows that the phase angle of the coated 304s samples with PDMS coatings after immersing for 1 day in the high frequency region is greater than that of the bare 304s sheet, implying that the PDMS coatings have good barrier properties after immersion in the electrolyte solution. After corrosion, only a time constant is observed when the 304s treated without and with the PDMS composite coatings (the content of alumina nanoparticles is less than 7.37%). Interestingly, when the loading alumina nanoparticles increased to 10.66%, the PDMS composite coating on surface of the 304s sheet exhibits a clear second time constant, indicating that diffusion corrosion began due to dispersive defects (gaps and holes) in the PDMS coatings, as shown in Fig. 4.

Subsequently, the Nyquist plots of the PDMS composite coatings were also provided to examine their anticorrosion performance. The capacitive loop of the bare 304s sheet is invisible as compared to those of the 304s sheets treated with the PDMS composite coatings, which can only be observed in the magnifying inset on the top right corner in Fig. 7c, indicating a remarkable charge-transfer behavior of the bare 304s sheet [61, 62]. But all the Nyquist plots of the 304s sheets treated with the PDMS composite coatings characterized by a similar shape of depressed semicircle, indicating a capacitive behavior after immersion of 24 h in 3.5 wt% NaCl solution, as shown in Fig. 7c. In the meantime, the diameter of the capacitive loop for the treated 304s sheets become large firstly, and then dramatically become small with an increase in loading amount of alumina nanoparticles, indicating that the corrosion resistance of the PDMS composite coating have the same trend as the change in the capacitive loop with content of alumina nanoparticles.

The potentio-dynamic polarization curves of the 304s sheets treated with PDMS composite coatings in electrolyte solution exhibit a similar cathodic polarization behavior, but their anodic polarization behavior is evidently different from the bare 304s, as revealed in Fig. 7d. Meanwhile, a sharp decrease in current density is obviously observed for the 304s sheets treated with PDMS composite coatings during anodic polarization, indicating that the corrosion resistance of the 304s sheets treated with PDMS composite coatings greatly increase as compared to that of the bare 304s sheet. In particular, the PDMS composite coating with 7.37% $Al_2O_3$ presents the lowest corrosion current density of $5.12\times10^{-6}$ A $cm^{-2}$ and the highest protection efficiency of 93.0%, indicating the optimal anticorrosion performance, as tabulated in Table 3. Moreover, corrosion potential ($E_{corr}$) shifts to the noble direction after treatment with different PDMS coatings, indicating that the PDMS composite coatings as protective layers may efficiently inhibit the anodic reaction and keep 304s sheets from corrosion. With an increasing loading amount of $Al_2O_3$ nanoparticles, the fluctuations in corrosion potential and current density of the 304s sheets treated with the PDMS composite coatings should be ascribed to the combined effect of synergy between silica and alumina nanoparticles and the dispersive defects of particles in PDMS composite coatings. As the loading amount of nano-alumina is less than 7.37%, the synergy between silica and alumina nanoparticles is favorable to reinforcing interaction between particles and PDMS chains. With the further increment in loading amount of nano-alumina, the more irregular protrusions and bumps made of the agglomerated alumina and silica particles are formed, contributing to reinforcing interaction between particles and particles and the increasing dispersive defects resulting from irregular distribution of the particles. Collectively, addition of the alumina nanoparticles into the PDMS composite coating plays a significant role in shifting the anodic curves to a greater extent toward the lower current density as compared to the cathodic curves.

Additionally, the EIS data of the 304s sheets with different PDMS composite coatings were further analyzed by

**Table 3** Corrosion potential ($E_{corr}$) and corrosion current ($I_{corr}$) parameters from the potentiodynamic polarization curves for all the 304s sheet specimens

| Sample | $E_{corr}$ (v) | $i_{corr}$ (A/cm$^2$) | Slope of anodic curves (V/dec) | Slope of cathodic curves (V/dec) | Protection efficiency (η%) |
|---|---|---|---|---|---|
| 304s | -0.429 | $7.34\times10^{-5}$ | 2.389 | 3.886 | / |
| SA-0 | 0.623 | $3.31\times10^{-5}$ | 9.399 | 0.187 | 54.9 |
| SA-1 | 0.55 | $1.11\times10^{-5}$ | 9.490 | 1.370 | 84.9 |
| SA-2 | 0.785 | $5.12\times10^{-6}$ | 8.605 | 2.271 | 93.0 |
| SA-3 | 0.464 | $1.68\times10^{-5}$ | 9.238 | 1.953 | 77.1 |

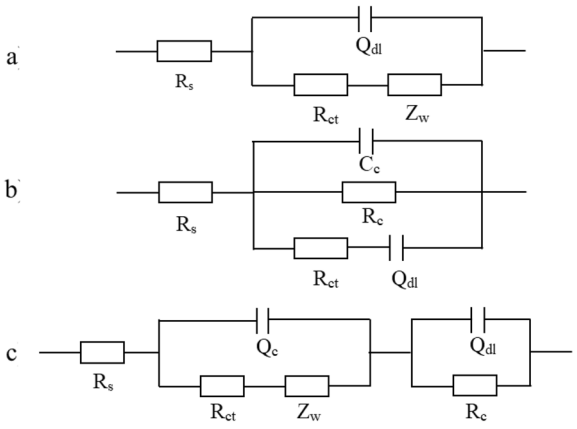


**Fig. 8** Equivalent electrical circuit model used for fitting the EIS measurements of 304s sheets treated with different PDMS composite coatings: **a** bare 304s, and the 304s sheets treated with **b** SA-0, **c** SA-1, SA-2 and SA-3, respectively. $R_s$, resistance of the electrolyte solution, $Q_{dl}$, constant phase element (CPE) of electrical double layer (EDL), $R_{ct}$, charge transfer resistance of EDL, $Q_c$, CPE of the PDMS composite coatings, $R_c$, resistance of the PDMS composite coatings, and $Z_w$, Warburg impedance

fitting with equivalent electrical circuits, which are present in Fig. 8. The chosen equivalent electrical circuit expresses high fitting quality ($\chi^2 < 0.01$). All parameters obtained by fitting the EIS data of the bare 304s sheet and the 304s sheets treated with different PDMS composite coatings are tabulated in Table 4. Notably, the PDMS composite coating with 7.37% alumina nanoparticles exhibits the largest $R_{ct}$ value among the other coatings with the increment in loadings of alumina nanoparticles, implicating that the lowest corrosion rate on the interface between electrolyte and metal. It is well-known that $R_c$ is closely related to surface microstructure and composition (holes, gaps, etc.) of the composite coating. Evidently, the coating with larger $R_c$ value can provides better protection effect. With an increase in loading content of alumina, $R_c$ value of the PDMS composite coatings decreases, reflecting more holes and gaps are forming in the PDMS composite coating during corrosion due to dispersive defects. Only the PDMS composite coating with 10.66% alumina nanoparticles exhibits the lowest $R_c$ value (lower than $10^6$ Ω cm$^2$), meaning the weakest barrier effect, as listed in Table 4. This result is also good agreement with the aforementioned SEM analysis. In short, from the point of view of the overall result, the PDMS composite coating with 7.37% alumina nanoparticles has the best corrosion resistance. This result also confirms that synergistic effect between silica and alumina nanoparticles could also block the diffusion channel of the oxygen and chloride ions causing corrosion due to barrier effects of PDMS composite coating [63].

## 4 Conclusions

In summary, a series of $Al_2O_3/SiO_2$/PDMS composite coatings were successfully fabricated and used for surface anticorrosion application of the 304s sheet through dip-coating method. The surface hydrophobicity, chemical compositions, microstructure, corroded morphologies, mechanical properties and stability of the untreated and treated 304s with the composite coatings are characterized, respectively. At the same time, the corrosion resistances of the 304s treated with and without the composite coatings are evaluated in corrosive medium (3.5 wt% NaCl solution) through potentiodynamic polarization tests and EIS techniques, respectively. The results show that the $Al_2O_3/SiO_2$/PDMS composite coatings have excellent mechanical properties and desirable thermal stability, and superior corrosion resistance compared to the PDMS coating without $Al_2O_3$ nanoparticles. It is noteworthy that the PDMS composite coating with 7.37% $Al_2O_3$ exhibits the best anticorrosion performance in 3.5 wt% NaCl solution due to excellent barrier between the 304s sheets and the corrosive medium. This work presents a simple and cost-efficient approach to exploiting hydrophobic composite coatings by use of binary nanoparticles (silica and alumina) and PDMS matrix, paving the way to the anticorrosion application of the $Al_2O_3/SiO_2$/PDMS composite coating for stainless steel in the future.

**Table 4** The parameters obtained from the electrochemical data, along with the equivalent circuit model used to fit the data, of all prepared coatings after immersion in 3.5 wt% NaCl solution for 1 day

| Samples | $R_s$ (Ω cm$^2$) | $C_c$ (F cm$^{-2}$) | $R_{ct}$ (Ω cm$^2$) | $R_c$ (Ω cm$^2$) | $Z_w$ (Ω cm$^2$) | $Q_c$ (F cm$^{-2}$) | $Q_{dl}$ (F cm$^{-2}$) |
|---|---|---|---|---|---|---|---|
| 304s | 14.8 | / | $2.3\times10^4$ | / | $2.8\times10^{-3}$ | / | $1.4\times10^{-6}$ |
| SA-0 | 13.9 | $3.8\times10^{-8}$ | $2.2\times10^5$ | $1.2\times10^6$ | / | / | $9.8\times10^{-7}$ |
| SA-1 | 13.3 | / | $4.6\times10^4$ | $1.2\times10^6$ | $9.4\times10^{-6}$ | $2.0\times10^{-6}$ | $1.3\times10^{-6}$ |
| SA-2 | 6.3 | / | $4.5\times10^5$ | $1.1\times10^6$ | $2.8\times10^{-6}$ | $6.0\times10^{-7}$ | $1.1\times10^{-6}$ |
| SA-3 | 27 | / | $2.4\times10^5$ | $3.3\times10^5$ | $4.9\times10^{-6}$ | $1.0\times10^{-6}$ | $1.0\times10^{-6}$ |

**Supplementary Information** The online version contains supplementary material available at https://doi.org/10.1007/s10904-022-02423-9.

**Acknowledgements** This work was supported by the National Natural Science Foundation of China (Grant Numbers 52173206 and 51503161), Scientific Research Foundation of Hubei Provincial Department of Education (Grant Number D20191702), the Open Project Program of High-Tech Organic Fibers Key Laboratory of Sichuan Province (Grant Number 20200518-1), Wuhan Textile University Training Program of Student Innovation and Entrepreneurship (Grant Numbers S202010495001 and S202010495003).

**Author Contributions** XS: Conceptualization, methodology, writing-original draft. JX: Data curation, formal analysis. JZ: Visualization, investigation. MS: Software. YL: Resources. PL: Project administration. DC: Writing review and editing, funding acquisition, supervision. HZ: Validation.

## Declarations

**Conflict of interest** The authors declare that they have no known competing financial interests or personal relationships that could have appeared to influence the work reported in this paper.

## References

1. K. Mallaiya, R. Subramaniam, S.S. Srikandan, S. Gowri, N. Rajasekaran, A. Selvaraj, Electrochim. Acta **56**, 3857 (2011)
2. N.A. Negm, N.G. Kandile, E.A. Badr, M.A. Mohammed, Corros. Sci. **65**, 94 (2012)
3. J. Zhao, D. Xu, M.B. Shahzad, Q. Kang, Y. Sun, Z. Sun, S. Zhang, L. Ren, C. Yang, K. Yang, Appl. Surf. Sci. **386**, 371 (2016)
4. X. Lv, X. Li, N. Li, H. Zhang, Y.-Z. Zheng, J. Wu, X. Tao, Surf. Coat. Technol. **358**, 443 (2019)
5. P. Khodaei, M. Shabani-Nooshabadi, M. Behpour, Prog. Org. Coat. **136**, 105254 (2019)
6. W. Zhao, R. Zhu, J. Jiang, Z. Wang, Appl. Surf. Sci. **484**, 307 (2019)
7. X. Li, D. Zhang, Z. Liu, Z. Li, C. Du, C. Dong, Nature **527**, 441 (2015)
8. T. Bellezze, G. Roventi, R. Fratesi, Electrochim. Acta **49**, 3005 (2004)
9. H. Yun, J. Li, H.-B. Chen, C.-J. Lin, Electrochim. Acta **52**, 6679 (2007)
10. S. Li, J. Fu, Corros. Sci. **68**, 101 (2013)
11. I.A. Kartsonakis, A.C. Balaskas, E.P. Koumoulos, C.A. Charitidis, G.C. Kordas, Corros. Sci. **57**, 30 (2012)
12. Y. Wang, D. Wei, J. Yu, S. Di, J. Mater. Sci. Technol. **30**, 984 (2014)
13. P.C. Okafor, X. Liu, Y.G. Zheng, Corros. Sci. **51**, 761 (2009)
14. M.A. Zavareh, A.A.D.M. Sarhan, P.A. Zavareh, B.B.A. Razak, W.J. Basirun, M.B.C. Ismail, Ceram. Int. **42**, 5203 (2016)
15. T. Xiang, Y. Han, Z. Guo, R. Wang, S. Zheng, S. Li, C. Li, X. Dai, ACS Sustain. Chem. Eng. **6**, 5598 (2018)
16. F. Yu, S. Chen, Y. Chen, H. Li, L. Yang, Y. Chen, Y. Yin, J. Mol. Struct. **982**, 152 (2010)
17. S. Yuan, S.O. Pehkonen, B. Liang, Y.P. Ting, K.G. Neoh, E.T. Kang, Corros. Sci. **52**, 1958 (2010)
18. A.F. Baldissera, C.A. Ferreira, Prog. Org. Coat. **75**, 241 (2012)
19. K.-C. Chang, M.-H. Hsu, H.-I. Lu, M.-C. Lai, P.-J. Liu, C.-H. Hsu, W.-F. Ji, T.-L. Chuang, Y. Wei, J.-M. Yeh, W.-R. Liu, Carbon **66**, 144 (2014)
20. T.K. Rout, A.V. Gaikwad, Prog. Org. Coat. **79**, 98 (2015)
21. D. Zhang, T. Yuan, G. Wei, H. Wang, L. Gao, T. Lin, J. Alloys Compd. **774**, 495 (2019)
22. H. Zhu, Y. Chen, H. Li, S.X. Wang, X. Li, Q. Zhu, Macromol. Rapid Commun. **40**, 1800252 (2019)
23. L. Ma, F. Chen, Z. Li, M. Gan, J. Yan, S. Wei, Y. Bai, J. Zeng, Composites B Eng. **58**, 54 (2014)
24. A. Ghanbari, M.M. Attar, J. Ind. Eng. Chem. **23**, 145 (2015)
25. M. Cai, X. Fan, H. Yan, Y. Li, S. Song, W. Li, H. Li, Z. Lu, M. Zhu, Chem. Eng. J. **419**, 130050 (2021)
26. S.A. Haddadi, E. Mehmandar, H. Jabari, A. Ramazani, R. Mohammadkhani, N. Yan, M. Arjmand, Composites Part B Eng. **212**, 108713 (2021)
27. Y. Qi, X. Li, Y. He, D. Zhang, J. Ding, A.C.S. Appl, Mater. Interfaces **11**, 202 (2019)
28. A. Trentin, A.L. Gasparini, F.A. Faria, S.V. Harb, F.C. dos Santos, S.H. Pulcinelli, C.V. Santilli, P. Hammer, Prog. Org. Coat. **138**, 105398 (2020)
29. S. Ammar, K. Ramesh, B. Vengadaesvaran, S. Ramesh, A. Arof, Prog. Org. Coat. **92**, 54 (2016)
30. C. Zhang, Y. He, F. Li, H. Di, L. Zhang, Y. Zhan, J. Alloys Compd. **685**, 743 (2016)
31. M.A. Deyab, A.A. Nada, A. Hamdy, Prog. Org. Coat. **105**, 245 (2017)
32. H. Huang, X. Huang, Y. Xie, Y. Tian, X. Jiang, X. Zhang, Prog. Org. Coat. **130**, 124 (2019)
33. W.F. Huang, Y.L. Xiao, Z.J. Huang, G.C.P. Tsui, K.W. Yeung, C.Y. Tang, Q. Liu, Mater. Lett. **258**, 126822 (2020)
34. W. Jiang, X. Jin, H. Li, S. Zhang, T. Zhou, H. Xie, Polym. Test. **82**, 106287 (2020)
35. G. Li, Z. Mai, X. Shu, D. Chen, M. Liu, W. Xu, Adv. Compos. Hybrid Mater. **2**, 254 (2019)
36. S. SharifiGolru, M.M. Attar, B. Ramezanzadeh, Prog. Org. Coat. **77**, 1391 (2014)
37. P. Xu, C. Lin, C. Zhou, X. Yi, Surf. Coat. Technol. **238**, 9 (2014)
38. D. Zhang, Y. Gou, Y. Liu, X. Guo, Surf. Coat. Technol. **236**, 52 (2013)
39. I.O. Arukalam, E.E. Oguzie, Y. Li, J. Colloid Interface Sci. **484**, 220 (2016)
40. J. Xie, J. Hu, X. Lin, L. Fang, F. Wu, X. Liao, H. Luo, L. Shi, Appl. Surf. Sci. **457**, 870 (2018)
41. D.-W. Li, H.-Y. Wang, Y. Liu, D.-S. Wei, Z.-X. Zhao, Chem. Eng. J. **367**, 169 (2019)
42. M.Y. Jiang, L.K. Wu, J.M. Hu, J.Q. Zhang, Corros. Sci. **92**, 118 (2015)
43. K. Kumar, S. Kumar, A. Kumar, R. Anant, R. Kumar, Polym. Compos. **39**, 2889 (2018)
44. D. Chen, C. Huang, X. Hu, Polym. Compos. **34**, 1041 (2013)
45. D. Chen, F. Chen, H. Zhang, X. Yin, X. Liu, Y. Zhou, Polym. Int. **64**, 1741 (2015)
46. D. Chen, F. Chen, X. Hu, H. Zhang, X. Yin, Y. Zhou, Compos. Sci. Technol. **117**, 307 (2015)
47. C. Jin, Z. Wang, A.A. Volinsky, A. Sharfeddin, N.D. Gallant, Polym. Test. **56**, 329 (2016)
48. W. Zhao, T. Li, Y. Li, D.J. O'Brien, M. Terrones, B. Wei, J. Suhr, X. Lucas Lu, J. Materiomics **4**, 157 (2018)
49. J. Song, Z. Peng, Y. Zhang, Chem. Eng. J. **391**, 123476 (2020)
50. C.-J. Weng, C.-H. Chang, I.L. Lin, J.-M. Yeh, Y. Wei, C.-L. Hsu, P.-H. Chen, Surf. Coat. Technol. **207**, 42 (2012)
51. F.S. Ertaş, R. Kaş, A. Mikó, Ö. Birer, Appl. Surf. Sci. **276**, 810 (2013)
52. U. Eduok, R. Suleiman, M. Khaled, R. Akid, Prog. Org. Coat. **93**, 97 (2016)
53. L. Hao, T. Yan, Y. Zhang, X. Zhao, X. Lei, S. Xu, F. Zhang, Surf. Coat. Technol. **326**, 200 (2017)

54. W.A. El-Said, A.S. Moharram, E.M. Hussein, A.M. El-Khawaga, Mater. Chem. Phys. **211**, 123 (2018)
55. R. Castaldo, M.S. de Luna, C. Siviello, G. Gentile, M. Lavorgna, E. Amendola, M. Cocca, J. Cultural Heritage (2020). https://doi.org/10.1016/j.culher.2020.01.016
56. X. Chen, S.F. Wen, T. Feng, X. Yuan, Prog. Org. Coat. **139**, 105374 (2020)
57. D. Sun, B.-B. Li, Z.-L. Xu, Desalination **322**, 159 (2013)
58. T.S. Radhakrishnan, J. Appl. Polym. Sci. **73**, 441 (1999)
59. D. Chen, Y. Liu, C. Huang, Polym. Degrad. Stab. **97**, 308 (2012)
60. M.F. Montemor, D.V. Snihirova, M.G. Taryba, S.V. Lamaka, I.A. Kartsonakis, A.C. Balaskas, G.C. Kordas, J. Tedim, A. Kuznetsova, M.L. Zheludkevich, M.G.S. Ferreira, Electrochim. Acta **60**, 31 (2012)
61. Y. Zhang, C. Wang, X. Dong, H. Jiang, T. Hu, C. Meng, C. Huang, Chem. Eng. J. **417**, 127964 (2021)
62. Y. Zhang, C. Wang, X. Chen, X. Dong, C. Meng, C. Huang, ACS Appl. Energy Mater. **4**, 9328 (2021)
63. C. Hu, Y. Li, T. Li, Y. Qing, J. Tang, H. Yin, L. Hu, L. Zhang, Y. Xie, K. Ren, Colloids Surf. A **585**, 124176 (2020)

**Publisher's Note** Springer Nature remains neutral with regard to jurisdictional claims in published maps and institutional affiliations.